*Article*

# Improved Method Based on Retinex and Gabor for the Surface Defect Enhancement of Aluminum Strips

**Qi Zhang [1], Hongqun Tang [1],*, Yong Li [2,3],*, Bing Han [2,3] and Jiadong Li [2,3]**

[1] Guangxi Key Laboratory of Processing for Nonferrous Metals and Featured Materials, Center of Ecological Collaborative Innovation for Aluminium Industry in Guangxi, School of Resources, Environment and Materials, Guangxi University, Nanning 530004, China

[2] State Key Laboratory of Rolling and Automation, Northeastern University, Shenyang 110819, China

[3] Guangxi Advanced Aluminum Processing Innovation Center Co., Ltd., Nanning 530007, China

* Correspondence: hqtang@gxu.edu.cn (H.T.); liyong.neu@163.com (Y.L.)

**Abstract:** Aiming at the problems of the blurred image defect contour and the surface texture of the aluminum strip suppressing defect feature extraction when collecting photos online in the air cushion furnace production line, we propose an algorithm for the surface defect enhancement and detection of aluminum strips based on the Retinex theory and Gobar filter. The Retinex algorithm can enhance the information and detail part of the image, while the Gobar algorithm can maintain the integrity of the defect edges well. The method first improves the high-frequency information of the image using a multi-scale Retinex based on a Laplacian filter, scales the original image and the enhanced image, and enhances the contrast of the image by adaptive histogram equalization. Then, the image is denoised, and texture suppressed using median filtering and morphological operations. Finally, Gobar edge detection is performed on the obtained sample images by convolving the sinusoidal plane wave and the Gaussian kernel function in the null domain and performing double-threshold segmentation to extract and refine the edges. The algorithm in this paper is compared with histogram equalization and the Gaussian filter-based MSR algorithm, and the surface defects of aluminum strips are significantly enhanced for the background. The experimental results show that the information entropy of the aluminum strip material defect image is improved from 5.03 to 7.85 in the original image, the average gradient of the image is improved from 3.51 to 9.51 in the original image, the contrast between the foreground and background is improved from 16.66 to 117.53 in the original image, the peak signal-to-noise ratio index is improved to 24.50 dB, and the integrity of the edges is well maintained while denoising. This paper's algorithm effectively enhances and detects the surface defects of aluminum strips, and the edges of defect contours are clearer and more complete.

**Keywords:** aluminum strip; image enhancement; Retinex; Laplacian; Gabor

## 1. Introduction

With the continuous development of machine vision, surface defect detection technology is used in a wide range of industries, such as wood, steel, semiconductors, pharmaceuticals, transportation, etc. In the aluminum alloy air cushion furnace production line for a continuous solution, quenching, annealing, aging, passivation, and other treatments of different series of aluminum alloys, the surface quality of aluminum strip heat treatment will also have many defects. The defects are caused by sticking to aluminum on the roller table and guide plate of the hot rolling mill, causing scratches on the hot-pressed strip or protruding sharp corners, or sticking to aluminum on the guide plate and flat roll of the cold rolling mill, which will result in scratch defects. Reel transportation, winding feeding crookedly, and the annealing of tower-shaped reels cause the relative dislocation of the reel layer and layer, and improper rolling tension causes layer-to-layer dislocation during rolling or unwinding, which will lead to friction. During cold rolling, the emulsion

is not blown out, so the emulsion is rolled into the reel. When the temperature of the emulsion is too high or the concentration is too large, the emulsion is bound on the strip, resulting in imprinting. There are also many common defects such as roll marks, pressed scratches, peeling, holes, air bubbles, insect marks, black bars, creases, bulging, and other defects. Due to the irregular size and shape of aluminum strip defects, blurred edges, and grain orientation during rolling, these factors can affect the extraction of defect features. Therefore, pre-processing the image for machine learning is a critical step in achieving efficient automation. The purpose of picture pre-processing [1] is to eliminate background information in the picture, retain useful defect information in the image, enhance the detectability of relevant information and maximize the simplification of defect contours, thus improving the accuracy of feature extraction and the reliability of recognition.

Image enhancement algorithms [2–5] in the field of aluminum strips image defect detection include histogram equalization [6,7], homomorphic filtering [8–10], bilateral filtering [11,12], and the Retinex algorithm [13–17]. Among them, histogram equalization can directly enhance the image's contrast, but it tends to cause excessive enhancement and severe distortion. Homomorphic filtering and bilateral filtering can remove noise well, but the details and edges of the image are seriously lost. Retinex theory is based on the human eye visual system perceiving no object brightness and color with constancy, which was proposed by Land et al. in 1985 based on the properties of the retina and cerebral cortex. Since then, Jobson et al. [18] proposed the single-scale Retinex algorithm (SSR) and the multi-scale Retinex algorithm (MSR) based on the central surround function, which further improved the Retinex theory. Jinxiang Maet al. [19] proposed enhancing the color recovery image algorithm with Gaussian filtering and bootstrap filtering, which effectively suppressed noise interference. Ping Wanget al. [20] proposed a Gabor filter [21,22]-based Retinex algorithm for the enhancement of low-illumination color images, replacing the Gaussian filter with a Gabor filter, which effectively reduces the halo and over-enhancement of images. Ruiqing Wu et al. [23] proposed a Retinex and Laplacian pyramid fusion method to fuse infrared. Yuanhong Qiu et al. [24] proposed a novel UISDI method using saliency detection and intrinsic image decomposition to detect various types of defects under inhomogeneous illumination accurately. Jiawei Zhang et al. [25] proposed a fuzzy measurement method to create and estimate model parameters, define the affiliation function, and test the acquired affiliation values of images. Guohua Liu et al. [26] proposed to construct a quadratic matrix by combining two-dimensional entropy and three feature maps, which can extract surface fabrics well.

This paper proposes an algorithm based on Retinex theory and Gabor for the surface defect enhancement of aluminum strips. The method first enhances the high-frequency information of the image using multi-scale Retinex based on the Laplacian filter, scales the enhanced image with the original image, and enhances the image's contrast by adaptive histogram equalization. Then, the defect image is denoised and suppressed with texture using median filtering and morphological operations. The obtained image defects are processed with Gobar edge detection and double-threshold segmentation. Then, clear image defect edge information is detected. The algorithm flow is shown in Figure 1.
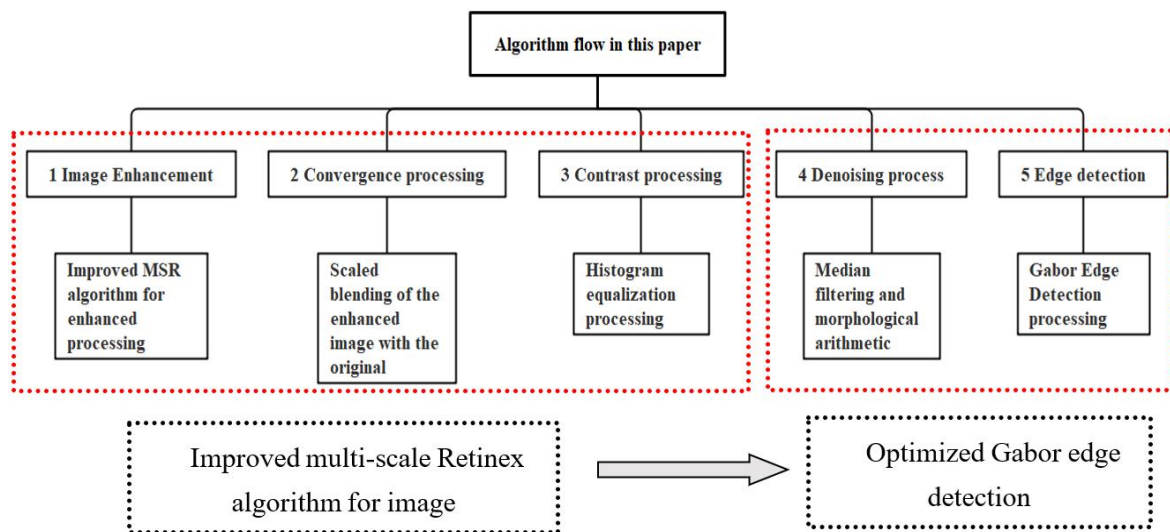
**Figure 1.** Flow chart of the algorithm in this paper.

## 2. Experimental Principles and Methods

### 2.1. Retinex Algorithm

Edwin, H.L. proposed the Retinex algorithm in 1963. Unlike the traditional linear and nonlinear ones that can only enhance some features of an image, the Retinex algorithm can achieve a balance in three aspects: compression of the dynamic range, edge enhancement, and color constancy, so it can meet the adaptive enhancement of different types of images. Retinex theory holds that, in the sun, the human eye can acquire the information reflected from the surface of an object under illumination, which is shown schematically in Figure 2.
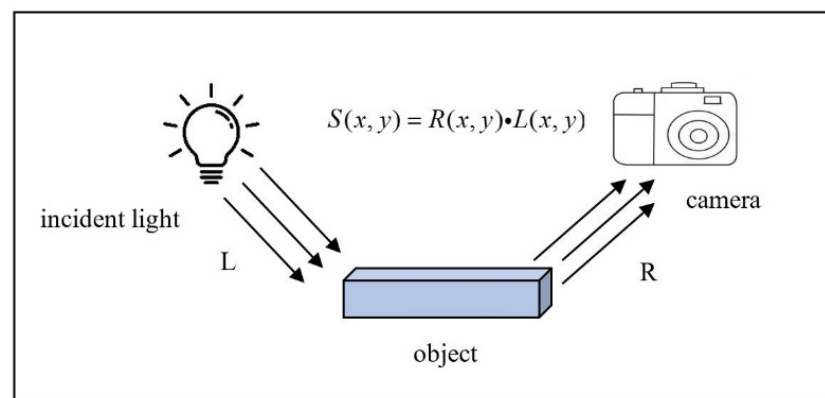


**Figure 2.** Schematic diagram of the Retinex algorithm.

The following equation can express the camera's information about the object's surface.

$$S(x,y) = R(x,y){\cdot}L(x,y) \tag{1}$$

where $R(x,y)$ denotes the reflected component of the object, and $L(x,y)$ indicates the irradiated element in the light. The essence of the Retinex algorithm process is to use some theory in the initial image to alter or reduce the impact of the incident image, ultimately preserving as much detail and as many edges of the object itself as possible. However, a simple mathematical process cannot solve the above equation directly to estimate its value. Depending on the luminance of the actual light source, many Retinex algorithms exist in the existing papers, which may have slightly different forms. Still, their essence is the same, and the general algorithm flow is shown in Figure 3.
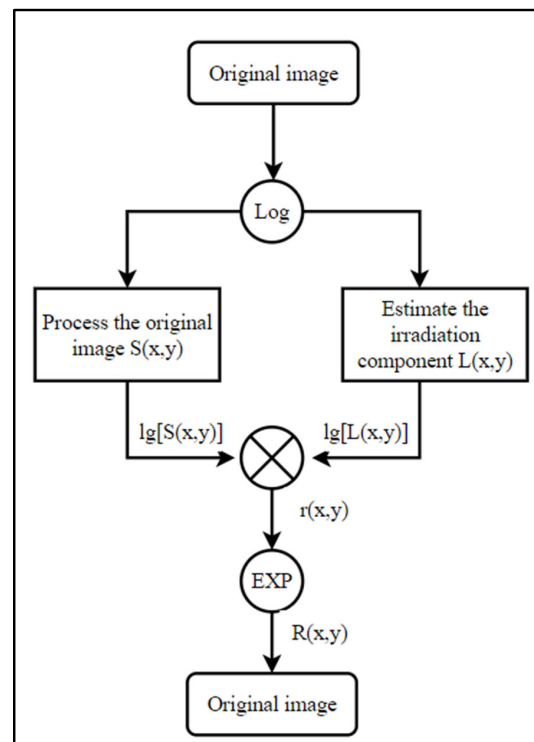
**Figure 3.** Processing flow of the Retinex algorithm.

However, the surface of an aluminum strip, which is the object of this paper, is highly reflective under the illumination of industrial light sources, and the defects on the surface range from raised bulges to undercutting scratches. This makes it very easy to detect defects in the reflective or diffuse areas, which makes it more difficult for Retinex to enhance the surface defects. In order to solve the influence of the reflective area when defects were detected by the Retinex algorithm, this paper uses a bright field camera and a dark field camera to collect the surface defects of an aluminum strip. The bright field is the area where the light source is at a certain angle to the object under study such that most of the light is reflected to the camera. The dark field is mainly the area outside the reflection area of the accepted light source. This alternate and complementary form can ensure that we collect the defect image in a manner that is more in line with the requirements. The angle of the bright field is set to 30°, and that of the dark field is set to 60°. The detailed parameters are shown in Figure 4.
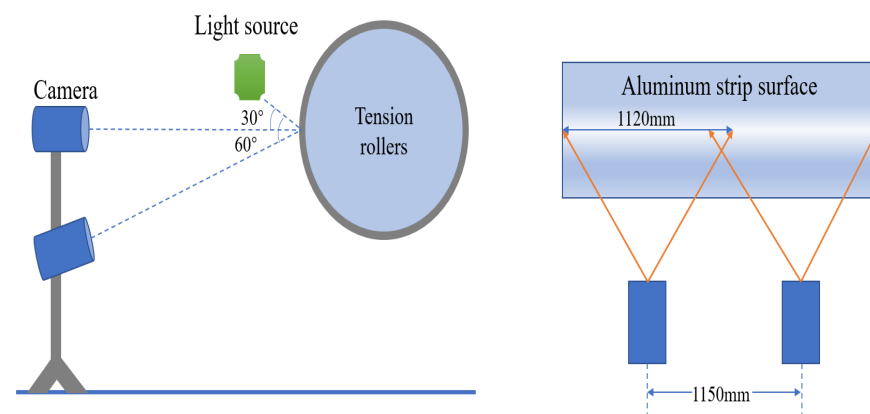


**Figure 4.** Surface inspection plan layout.

*2.2. Improved Retinex-Based Image Defect Enhancement Algorithm*

2.2.1. Laplacian Filter

The Laplace operator is a second-order differential operator [27,28]. Its essence is an isotropic filter. That is, the response of the filter has nothing to do with the mutation direction of the filtered image, and it is widely used in high-frequency information and image detail processing algorithms. Its image in the spatial domain of the defining function is $S(x,y)$. Perform the Laplace transformation as shown in the following equation.

$$\nabla^2 S(x,y) = \frac{\partial^2 S(x,y)}{\partial^2 x} + \frac{\partial^2 S(x,y)}{\partial^2 y} \tag{2}$$

Perform the discretization as follows [29].

$$F(x,y) = \nabla^2 S(x,y) = S(x+1,y) + S(x-1,y) + S(x,y+1) + S(x,y-1) - 4S(x,y) \tag{3}$$

The result of its filter kernel in the four directions of up, down, left, and right is the same as 1, and it has no direction. Modify it so that the mask also has this property in the 45-degree direction. The extended definition is shown in Figure 5.
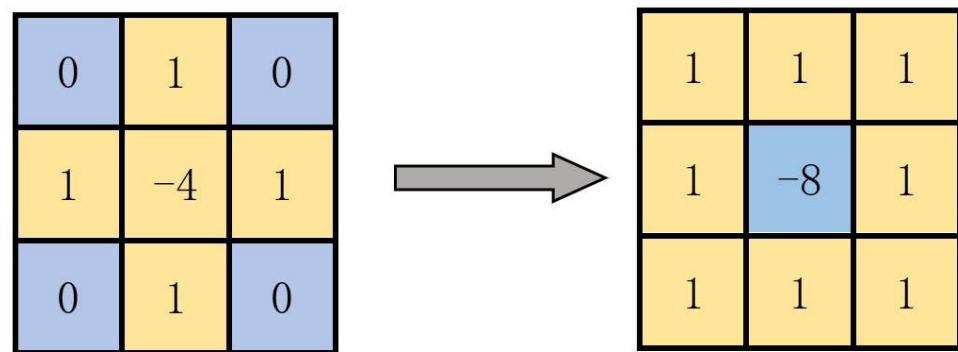


**Figure 5.** Improvement of the filter kernel.

2.2.2. Enhancement Algorithm of Retinex Based on Laplacian Filtering

Based on the theory of Retinex, SSR, MSR, and Multi-scale Retinex with Color Restoration (MSRCR), RGB images are derived. The primary method is to replace the incident component with a Gaussian low-pass filter $G(x,y)$ and convolve it with the original image to optimize the algorithm [14].

$$\begin{aligned} r(x,y) &= \log R(x,y) = \log[S(x,y)/L(x,y)] \\ &= \log S(x,y) - \log[G(x,y) * S(x,y)] \end{aligned} \tag{4}$$

where $r(x,y)$ is denoted as the output image, $G(x,y)$ is the Gaussian low-pass filter, i.e., the center-surround function, $S(x,y)$ is the original image, and * is the convolution symbol. The two-dimensional Gaussian filter function (with the center point as the origin) can be expressed as.

$$G(x,y) = \frac{1}{2\pi\sigma^2} e^{-(x^2+y^2)/2\sigma^2} \tag{5}$$

Among them, the influence factor of the Gaussian filter function depends mainly on selecting A. As A decreases, the image will retain more details, but it will lead to color imbalance; as A increases, the color enhancement effect of the image will be significantly improved, but the details and its defective edges will be blurred.

Since SSR has a difficult time finding a balance between dynamic range compression and color sense uniformity, Jobson et al. also proposed the multi-scale Retinex, and the processed image is obtained by weighting based on SSR, which is calculated as follows [15].

$$r(x,y) = \sum_i^k w_i \{\log S(x,y) - \log[G_i(x,y) * S(x,y)]\} \tag{6}$$

where $k$ is the number of Gaussian center-surround functions, to ensure that the SSR has high, medium, and low scale dimensions simultaneously, $k$ usually takes the value of 3. Therefore, we have $W_1 = W_2 = W_3 = 1/3$.

The central surround function of the traditional Retinex algorithm is a Gaussian filter, which is a linear filter. Its effect is to reduce the sharp transformation of the image, making the image more smooth, which is better for suppressing the noise obeying the normal distribution but leads to the blurring of the image, producing halos and artifacts. In response to the problems generated by the Gaussian filter, some scholars proposed an improved Retinex scheme based on bilateral filtering, whose core idea is to use bilateral filtering instead of Gaussian filtering, but the processing of images will generate a lot of high-frequency information, eliminating the noise while losing the details of the edges. Some scholars also propose Gabor filtering based on Gabor to replace Gaussian filtering in Retinex; the disadvantage is that the processing speed of the image will be significantly slowed down due to the large computational effort of the Gabor algorithm. The comparison of different improved Retinex algorithmis shown in Table 1.

**Table 1.** Comparison of different improved Retinex algorithms.

| Algorithm | Center Surround Function (Filters) | Disadvantages | Experimental Results |
|---|---|---|---|
| Multi-Scale Retinex Algorithm [18] | Gaussian filter function | Prone to halation, over-enhancement | The image is blurry and dark |
| Retinex based on bilateral filtering | Bilateral filtering function | Saves too much high-frequency information | Noise can be removed, but details are lost |
| Retinex based on the Gabor filter [20] | Gabor filter function | Too much calculation | Long calculation time |

Therefore, the Laplace filter is used in this paper. It is a second-order differential operator that focuses more on the abrupt changes in the gray scale in the image. The original image and the Laplace image are fused together to achieve the effect of sharpening the image and making the edge details of image defects more prominent. Using the Laplacian operator instead of Gaussian filtering as the central winding function of the MSR algorithm can keep the image edges well. The Laplacian-based multi-scale Retinex algorithm is formulated.

$$r(x,y) = \sum_i^k w_i \{\log S(x,y) - \log[F_i(x,y) * S(x,y)]\} \tag{7}$$

where $K$ is the number of weights, $w$ denotes the corresponding weight value, and $F_i(x,y)$ denotes the center-surround function using the Laplace operator.

### 2.3. Gabor-Based Edge Detection Algorithm for Image Defects

2.3.1. Median Filtering and Morphological Operations for Noise Cancellation

Median filtering is a nonlinear image smoothing and denoising algorithm that can effectively overcome the blurring of image details caused by linear filtering. The principle of its processing image is that a sliding window containing an odd number of points is used, and the median of the gray values in the window is used instead of the gray

values of the center points. The median filtering window used in this paper is for a square (3 × 3 window), defined as.

$$h(x,y) = med\{f(x_i, y_i)\} \ (i,j) \in M \tag{8}$$

where $h(x,y)$ is the output image, $f(x_i, y_i)$ denotes the gray value of the pixel $(x_i, y_i)$ at each point of the image, and $M$ is the template window.

Morphological operations [30] are a series of operations performed on the defects of the image, including expansion, erosion, binarization, open operations, closed operations, top-hat algorithms, etc. Due to the existence of small cavities and fractures before the defects on the surface of the aluminum strip, for example, the image defects are slender and very narrow. The closed operation can eliminate the isolated points of the neighboring points and achieve the effect of noise removal, which can bridge the narrow interruptions and slender gaps to achieve a smooth contour of the object. Therefore, in this paper, we use the closed operation to expand the boundary of the connected domain and connect the two adjacent connected domains. Then, we perform the erosion operation to reduce the expansion of the boundary of the connected domain and increase the area caused by the expansion operation. The specific principle is as follows.

Expansion: The operation of finding the local maximum that causes the highlighted area of the image to grow gradually with the following mathematical expression.

$$dst(x,y) = \max src(x + x', y + y') \tag{9}$$

where the maximum value in the region $(x + x', y + y')$ around $(x,y)$ replaces the value of $(x,y)$.

### 2.3.2. Gabor-Based Image Edge Detection

Gabor filters are linear filters commonly used for image edge detection. Gabor is very similar to the human visual system, and the difference in residuals between the two is extremely small. It has a remarkable effect in extracting the local spatial and frequency domain information of the target. The Gabor filter is sensitive to the edge information of the acquired image, i.e., high-frequency information has a good orientation selection and scale selectivity and an adaptability to illumination transformations. In the spatial domain, a Gabor is a Gaussian kernel function that is modulated by a sinusoidal plane.

The impulse response of a Gabor filter [31,32] can be defined as a sine wave (for a two-dimensional Gabor filter, it is a sinusoidal plane wave) multiplied by a Gaussian function. Due to the multiplicative convolution property, the Fourier transform of the impulse response of the Gabor filter is the convolution of the Fourier transform of its summation function and the Fourier transform of the Gaussian function. The filter consists of a real and an imaginary part, which are orthogonal to each other.

Plural expressions [31]:

$$g(x,y : \lambda, \psi, \sigma, \gamma) = \exp\left(-\frac{x^2 + \gamma^2 y'^2}{2\sigma^2}\right)\exp\left(i\left(2\pi\frac{x'}{\lambda} + \psi\right)\right) \tag{10}$$

Real number component [32]:

$$g(x,y : \lambda, \psi, \sigma, \gamma) = \exp\left(-\frac{x^2 + \gamma^2 y'^2}{2\sigma^2}\right)\cos\left(\left(2\pi\frac{x'}{\lambda} + \psi\right)\right) \tag{11}$$

Imaginary part:

$$g(x,y : \lambda, \psi, \sigma, \gamma) = \exp\left(-\frac{x^2 + \gamma^2 y'^2}{2\sigma^2}\right)\sin\left(\left(2\pi\frac{x'}{\lambda} + \psi\right)\right) \tag{12}$$

where $x'$ and $y'$ are calculated as follows.

$$x' = x \cos \theta + y \sin \theta \tag{13}$$

$$y' = -x \sin \theta + y \cos \theta \tag{14}$$

In the above equation, $\lambda$ denotes the wavelength of the cosine function in pixels, $\theta$ denotes the direction of the parallel stripes of the Gabor function, $\psi$ denotes the phase deviation, and $\gamma$ denotes the aspect ratio, which determines the shape of the Gabor.

Gabor's specific edge detection steps: first, establish Gabor filter banks; choose three scale parameters: 6, 9, 12, and 15. Gabor filters havean angular interval of $\pi/4$, i.e., 0, $\pi/4$, $\pi/2$, and $3\pi/4$, thus forming 16 Gabor filters, as shown in Figure 6. The scales of the first to fourth rows are 6, 9, 12, and 15, in order. The first to fourth columns indicate different angles: 0, $\pi/4$, $\pi/2$ and $3\pi/4$, respectively.
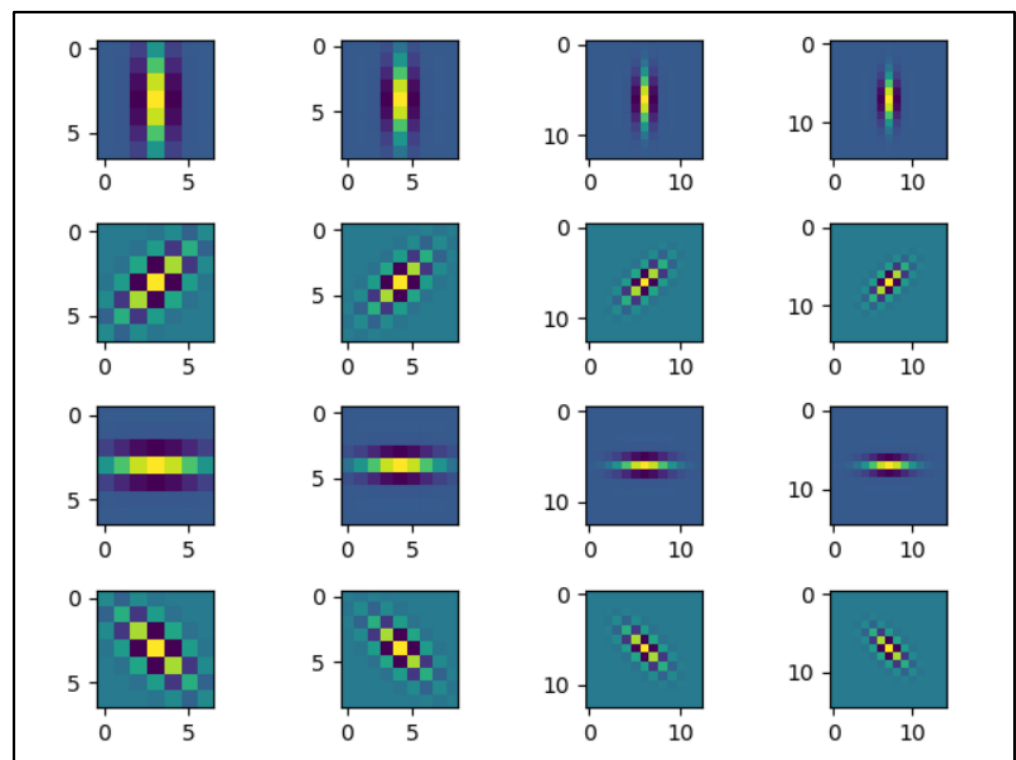


**Figure 6.** Schematic diagram of the choice of the scale and orientation of the Gabor filter.

Then, Gabor filter banks are convolved with each image block in the null domain, and each image block can obtain 24 filter outputs, which are images of image block size. If they are directly used as feature vectors, the dimension of the feature space will be large. So, they need to be compressed, and the 24 outputs of each image block after the Gabor filter banks are to be compressed into a $24 \times 1$ column vector as the image block texture features. The specific parameters of Gabor are listed in Table 2.

**Table 2.** The meaning and value of Gabor parameters.

| Parameter | Physical Significance | Value |
|---|---|---|
| (x, y) | Pixel coordinate position | (0,0) |
| $\lambda$ | Wavelength affects the filtering scale | $\geq 2$ |
| $\theta$ | Kernel function tilt angle | $(0, 2\pi)$ |
| $\psi$ | Phase Shift | $(-\pi, \pi)$ |
| $\gamma$ | Space Aspect Ratio (Aspect Ratio) | 0.5 |
| $\sigma$ | Bandwidth | $2\pi$ |

## 3. Experimental Results and Analysis

This work has been applied to the development of an online surface inspection tester for aluminum strip air cushion furnace lines. The aluminum strip surface inspection system consists mainly of process conditions and equipment conditions. The process conditions include, in particular, the location of the detection of defects in the aluminum strip located on the surface of the tension roll. The detection method continuous online. The detection area is the upper surface of the coil and the lower surface of the coil. The maximum speed of the aluminum strip is: 60 m/min. The lateral resolution and longitudinal resolution of the camera is less than 0.2 mm/pixel. The working environment temperature is stable from 0 to 50 °C, and the detection method of the site is a combination of bright field and dark field detection. Specific parameters are shown in Table 3. The experimental equipment mainly includes the CMOS line array camera (bright field + dark field), LED light source, graphics workstation, controller, driver, two-phase stepper motor, power supply, equipment stand, etc.This is shown in Figure 7.

**Table 3.** Experimental process parameters.

| Detection Location | Tension Roller Surface | Collection Method | Continuous, Online |
|---|---|---|---|
| Detection area | Coil upper and lower surfaces | Maximum strip speed | 80 m/min |
| Camera horizontal resolution | ≤0.2 mm/pixel | Camera vertical resolution | ≤0.2 mm/pixel |
| Working environment temperature | 0~50 °C | Detection method | Bright field and dark field |
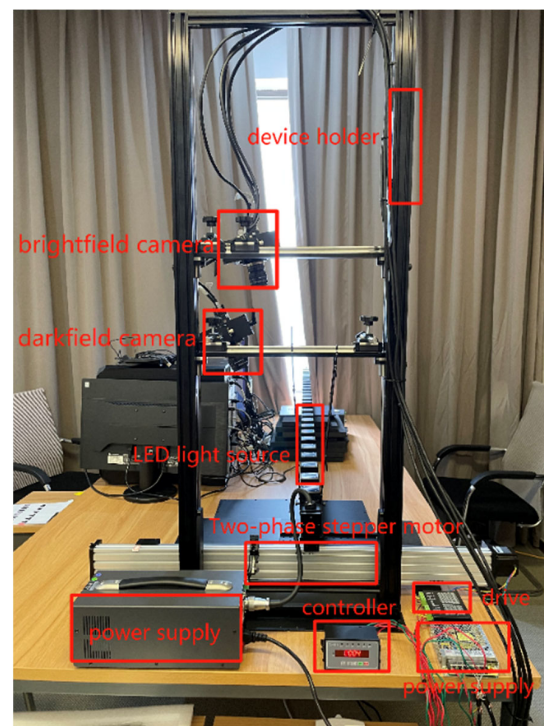


**Figure 7.** The experimental setup.

The experimental environment of this paper is Intel(R) Xeon(R) Gold 5218 CPU@2.30 GHz; the memory is 64 G; the operating system is Windows 10; algorithm verification is implemented using MATLAB2014a and PyCharm2021. To check the effectiveness of the enhancement and edge detection of the surface defects of aluminum strips based on the

improved Retinex algorithm and Gabor filter, in this paper, the data of the images of the surface defects of aluminum strips are obtained from Guangxi Nanan Aluminum Processing Co. For the typicality of aluminum alloy surface defects, this paper selects the surface defects of aluminum strips taken under three different environments (bright field and dark field), which are blot (a), lacerate (b), and scratch (c) in a bright field and blot (d), lacerate (e), and scratch (f) in a dark field. Thisis shown in Figure 8.
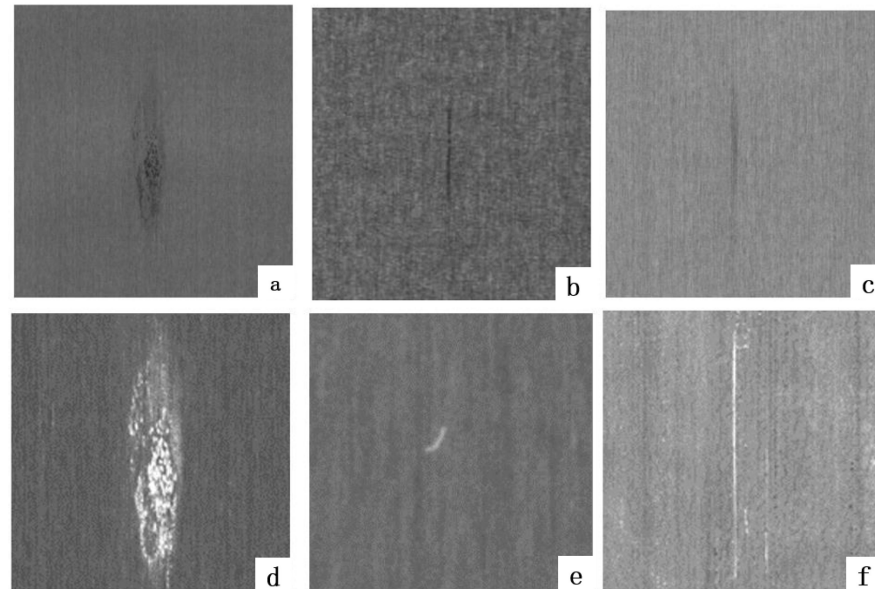


**Figure 8.** Sample diagram of defects in aluminum strips: (**a,d**) blot; (**b,e**) lacerate; (**c,f**) scratch.
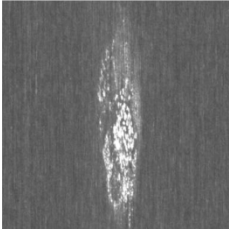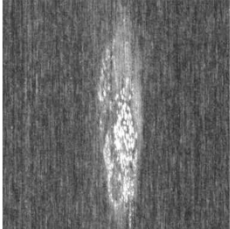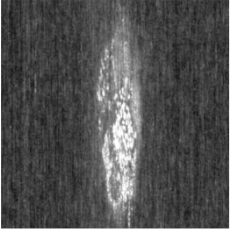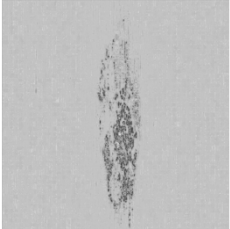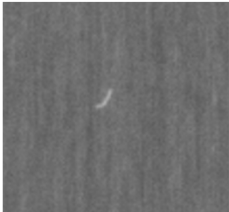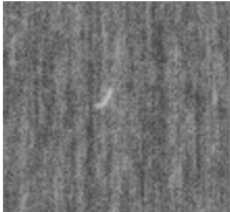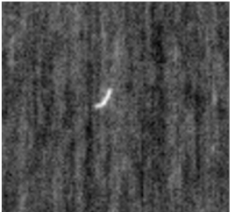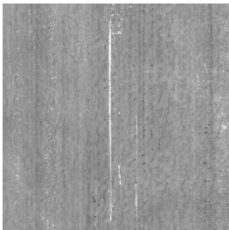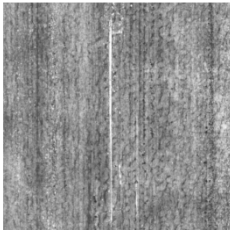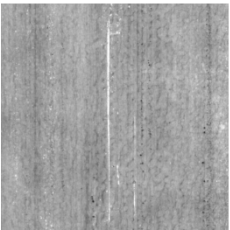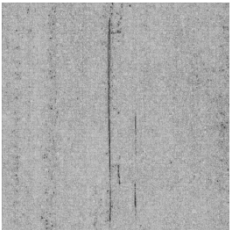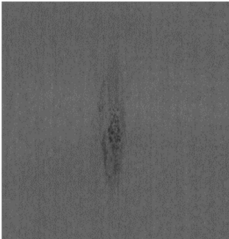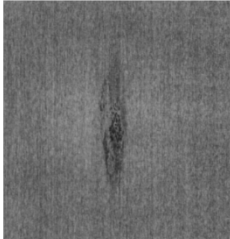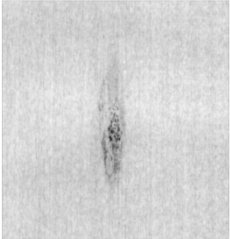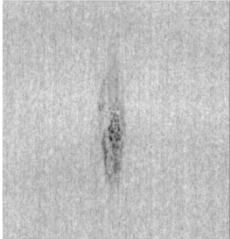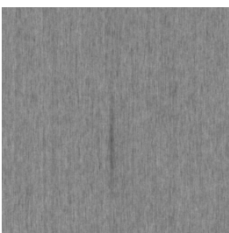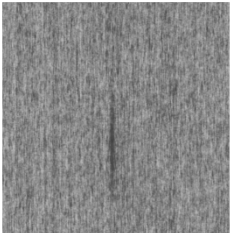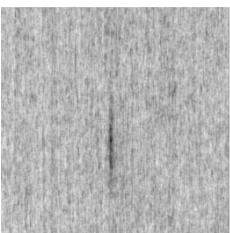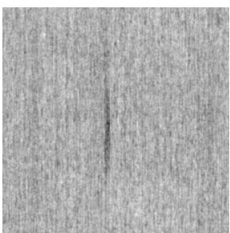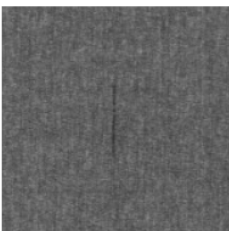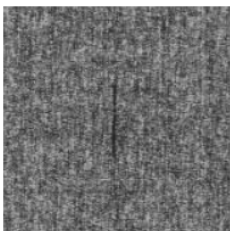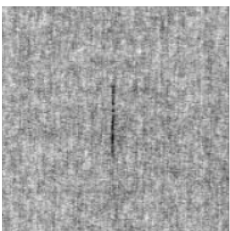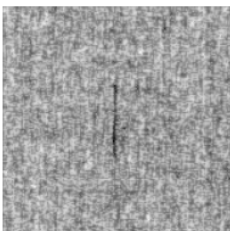
### 3.1. Improved Multi-Scale Retinex Algorithm for Image Enhancement Results

All surface defect images of aluminum strips were processed and compared with local histogram equalization (contrast set to 2; slider size set to $4 \times 4$) and the Retinex algorithm based on Gaussian filtering ($k = 3$), and they were analyzed using the algorithm in this paper. The settings of the experimental parameters of the algorithm in this paper are: the Gaussian kernel in the MSR algorithm takes the value of 40, and the weight is $1/3$; the angular interval of the Gabor filter is $\pi/8$, which is $0$, $\pi/8$, $\pi/4$, $3\pi/8$, $\pi/2$, $\pi/4$, $5\pi/8$, $3\pi/4$, and $7\pi/8$; the default of the Gabor kernel is the origin position, which is $(0, 0)$; $1/\lambda$ is the center frequency of Gabor. The effect comparison plots are shown in Table 4.

From the experimental results in Figure 9, it is obvious that the original defect image of the aluminum strip has the disadvantages of a low brightness and blurred defect edges, which is not conducive to feature extraction and detection. After adaptive histogram equalization, although the contrast and brightness of defects can be improved, it will also attract a lot of noise, seriously distort the background, and cover the details. In the Retinex algorithm processed by Gaussian filtering, the image's noise is much less than that of the histogram equalization, and the edge information of the defects is reduced due to Gaussian filtering, which affects the extraction of edge details. Finally, the algorithm in the first stage of this paper—Retinex processing based on improved Laplace filtering—has precise image details and a high contrast, which facilitates the detection of defects. To further illustrate the problem, the histogram of the enhancement effect of various algorithms on the scratch defect images of aluminum strips is judged by Figure 6. "a" indicates the original image, the pixel values are mainly concentrated between 95 and 105, and the overall image is dark. "b" is the image processed by local histogram equalization. Although the pixels are partially equalized, the brightness is still low. "c" is the Gaussian-filtered Retinex algorithm, the brightness of the image decreases instead, and the pixel values are mainly concentrated in the range of 50–100. "d"is the Retinex algorithm with improved Laplacian

filtering, the brightness of the image is significantly improved, and the concentrated pixels are concentrated in 200.

**Table 4.** Comparison of the enhancement effect of different algorithms on defects in aluminum strips.

| Method<br>Defects | Original Image | CLAHE | MSR | Improve Retinex |
|---|---|---|---|---|
| Blot<br>(DF) | | | | |
| Lacerate<br>(DF) | | | | |
| Scratch<br>(DF) | | | | |
| Blot<br>(BF) | | | | |
| Lacerate<br>(BF) | | | | |
| Scratch<br>(BF) | | | | |
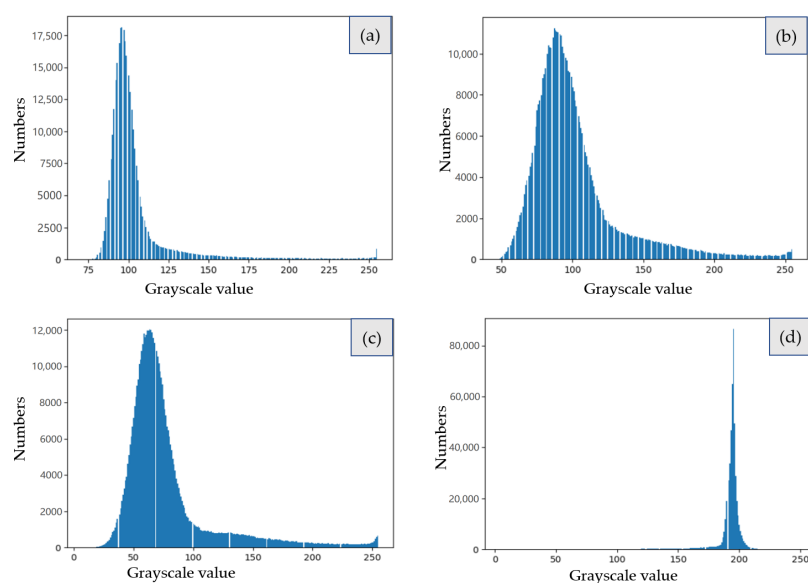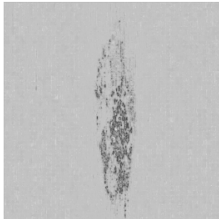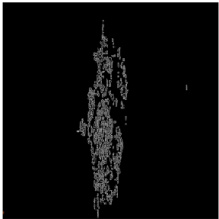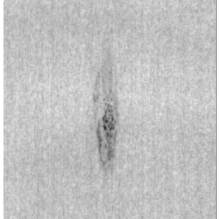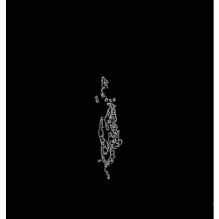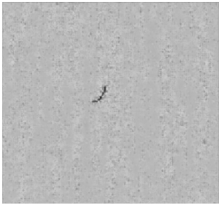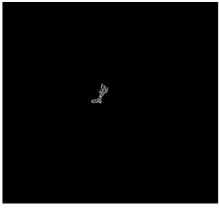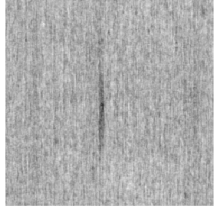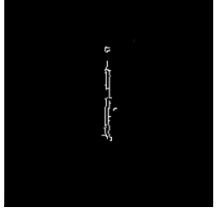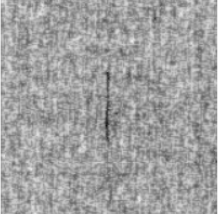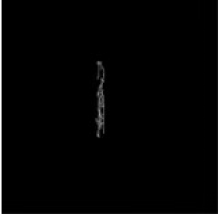
**Figure 9.** Defect image histogram: (**a**) initial image; (**b**) histogram equalization; (**c**) MSR; (**d**) this article's algorithm.

*3.2. Optimizing Gabor Edge Detection Results*

After the Retinex algorithm processing of aluminum strip surface defects by Laplace filtering, the further detection of the edges of the defects is required. First, the original image is processed by median filtering and morphological operations. The Gabor filter can effectively suppress the blurred edges existing in the collected aluminum strip photos, which improves the edge continuity of defects and has better robustness for traditional aluminum strip processing on different occasions. The experimental results are shown in Table 5.
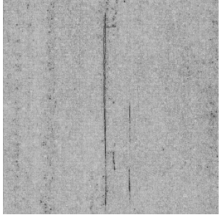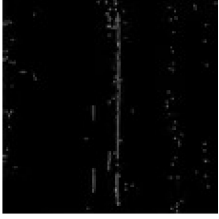
**Table 5.** Aluminum strip surface defect edge extraction.

| | Image Enhancement | Edge Detection | Image Enhancement | Edge Detection |
|---|---|---|---|---|
| Blot |  |  |  |  |
| Lacerate |  |  |  |  |
| Scratch |  |  |  |  |

Finally, common image evaluation metrics [33,34], such as the information entropy, average gradient, contrast ratio, and peak signal-to-noise ratio, are used to evaluate the effectiveness of different algorithms in processing images. The information entropy (H) is used to express the amount of useful information contained in an image. The larger the information entropy is, the more information is contained in the image and its mathematical expression.

$$H = -\sum_{i=0}^{255} P_i \log P_i \tag{15}$$

where $P_i$ denotes the proportion of pixels with the gray value in the image.

The peak Signal-to-Noise Ratio (*PSNR*) is expressed as:

$$PSNR = 10 \log 10 \left( \frac{(MAX_x)^2}{MSE} \right) \tag{16}$$

The average gradient (*AG*) is mainly used to measure the image contrast. The larger its value, the higher the image contrast, and its mathematical expression isas follows.

$$AG = \frac{1}{MN} \sum_{i=1}^{M} \sum_{j=1}^{N} \sqrt{\frac{\left(\frac{\partial f}{\partial x}\right)^2 + \left(\frac{\partial f}{\partial y}\right)^2}{2}} \tag{17}$$

The objective metrics of the algorithms are compared in Table 6.

**Table 6.** Evaluation criteria of various algorithms for processing scratch defect images.

| Algorithm | IE | AG | CR | PSNR |
|---|---|---|---|---|
| Original image | 5.0288 | 3.5176 | 16.6552 | 0 |
| CLAHE | 6.2429 | 9.2792 | 115.4192 | 15.5364 |
| MSR | 6.1802 | 8.4166 | 96.5652 | 14.2221 |
| Improved algorithm | 7.8544 | 9.5079 | 117.5332 | 24.50183 |

It can be seen in Table 3 that the local histogram equalization mainly enhances the contrast and average gradient of the image itself, making the foreground and background more obvious. However, at the same time, it contains less detailed parts and has a lower peak signal-to-noise ratio, which can lead to poorer visual effects. The Retinex algorithm is based on traditional Gaussian filtering. Although the contrast will likewise make the image defective to some extent, the overall level, both in terms of sharpness and/or the information contained, is lower than that of the algorithm in this paper. The information entropy of the algorithm in this paper is improved from 5.03 to 7.85 in the original image. The average gradient of the image is improved from 3.51 to 9.51 in the original image, the contrast between the foreground and background is improved from 16.66 to 117.53 in the original image, the peak signal-to-noise ratio index is improved to 24.50 dB, and the integrity of the edges is well maintained while denoising. The brightness, contrast, and detail contour of the image are significantly enhanced, and the comprehensive optimization effect is obvious.

In order to react to whether the algorithm matches between the calculated response speed and the actual running speed of the aluminum strip in the process of enhancing the defects, the device diagram shown in Figure 7 is made in the experiment, which mainly includes the parameters of the motion device controlled by the motor to control the speed and the camera to control the shooting device. The speed of the motor is 60 m/min, and the power consumption is about 100 W. The acquisition process of the CMOS line array camera is divided into bright field and dark field, and the specific parameter settings are shown in Table 7. The experimental results show that the developed algorithm basically matches the response speed in the experimental state. The field environment basically matches with our

experimental environment. The developed software can give a real-time response during the strip processing.

**Table 7.** Camera's specific parameters.

|  | **Acquisition Line Rata** | **Exposure Time** | **Gain** |
| --- | --- | --- | --- |
| Bright field | 800 Hz | 12 μs | 2 dB |
| Dark field | 1100 Hz | 12 μs | 2 dB |

## 4. Conclusions

Based on the online photo collection of the aluminum strip air cushion furnace production line, the image defect contour is blurred and the aluminum strip surface texture inhibits the defect feature extraction. An improved Retinex algorithm and Gabor algorithm are proposed to enhance and detect the surface defects of aluminum strips. The method first enhances the high-frequency information of the image using the multi-scale Retinex based on the improved Laplacian filter, scales the obtained image with the original image, and enhances the contrast of the image by adaptive histogram equalization. Then, the images are denoised and the texture is suppressed using median filtering and morphological operations. Gobar edge detection processing is performed on the samples, and then clear defect edge information is obtained.

**Institutional Review Board Statement:** Not applicable.

**Informed Consent Statement:** Not applicable.

**Data Availability Statement:** Not applicable.

**Conflicts of Interest:** The authors declare no conflict of interest.

## References

1. Guo, Y.M.; Liu, Y.; Oerlemans, A.; Lao, S.Y.; Wu, S.; Lew, M.S. Deep learning for visual understanding: A review. *Neurocomputing* **2016**, *187*, 27–48. [CrossRef]
2. Xu, Y.; Wen, J.; Fei, L.K.; Zhang, Z. Review of Video and Image Defogging Algorithms and Related Studies on Image Restoration and Enhancement. *IEEE Access* **2016**, *4*, 165–188. [CrossRef]
3. Tang, B.; Chen, L.; Sun, W.; Lin, Z.K. Review of surface defect detection of steel products based on machine vision. *IET Image Process.* **2022**, 1–20. [CrossRef]
4. Chen, Y.; Peng, X.; Kong, L.B.; Dong, G.X.; Remani, A.; Leach, R. Defect inspection technologies for additive manufacturing. *Int. J. Extrem. Manuf.* **2021**, *3*, 022002. [CrossRef]
5. Buades, A.; Coll, B.; Morel, J.M. A review of image denoising algorithms, with a new one. *Multiscale Model. Simul.* **2005**, *4*, 490–530. [CrossRef]
6. Vijayalakshmi, D.; Nath, M.K. A novel multilevel framework based contrast enhancement for uniform and non-uniform background images using a suitable histogram equalization. *Digit. Signal Process.* **2022**, *127*, 103532. [CrossRef]

7. Zhang, W.; Dong, L.; Xu, W. Retinex-inspired color correction and detail preserved fusion for underwater image enhancement. *Comput. Electron. Agric.* **2022**, *192*, 106585. [CrossRef]

8. Al Sobbahi, R.; Tekli, J. Low-Light Homomorphic Filtering Network for integrating image enhancement and classification. *Signal Process. Image Commun.* **2022**, *100*, 116527. [CrossRef]

9. Yugander, P.; Tejaswini, C.H.; Meenakshi, J.; Kumar, K.S.; Varma, B.V.N.S.; Jagannath, M. MR Image Enhancement using Adaptive Weighted Mean Filtering and Homomorphic Filtering. *Procedia Comput. Sci.* **2020**, *167*, 677–685. [CrossRef]

10. Xiao, L.; Li, C.; Wu, Z.; Wang, T. An enhancement method for X-ray image via fuzzy noise removal and homomorphic filtering. *Neurocomputing* **2016**, *195*, 56–64. [CrossRef]

11. Riya; Gupta, B.; Lamba, S.S. Structure-aware adaptive bilateral texture filtering. *Digit. Signal Process.* **2022**, *123*, 103386. [CrossRef]

12. Caraffa, L.; Tarel, J.P.; Charbonnier, P. The Guided Bilateral Filter: When the Joint/Cross Bilateral Filter Becomes Robust. *IEEE Trans. Image Process.* **2015**, *24*, 1199–1208. [CrossRef]

13. Jang, J.H.; Kim, S.D.; Ra, J.B. Enhancement of Optical Remote Sensing Images by Subband-Decomposed Multiscale Retinex With Hybrid Intensity Transfer Function. *IEEE Geosci. Remote Sens. Lett.* **2011**, *8*, 983–987. [CrossRef]

14. Fu, Q.; Jung, C.; Xu, K. Retinex-Based Perceptual Contrast Enhancement in Images Using Luminance Adaptation. *IEEE Access* **2018**, *6*, 61277–61286. [CrossRef]

15. Aguirre-Castro, O.A.; García-Guerrero, E.E.; López-Bonilla, O.R.; Tlelo-Cuautle, E.; López-Mancilla, D.; Cárdenas-Valdez, J.R.; Olguín-Tiznado, J.E.; Inzunza-González, E. Evaluation of underwater image enhancement algorithms based on Retinex and its implementation on embedded systems. *Neurocomputing* **2022**, *494*, 148–159. [CrossRef]

16. Zotin, A. Fast Algorithm of Image Enhancement based on Multi-Scale Retinex. *Procedia Comput. Sci.* **2018**, *131*, 6–14. [CrossRef]

17. Wang, W.; Wu, X.; Yuan, X.; Gao, Z. An Experiment-Based Review of Low-Light Image Enhancement Methods. *IEEE Access* **2020**, *8*, 87884–87917. [CrossRef]

18. Jobson, D.J.; Rahman, Z.; Woodell, G.A. A multiscale retinex for bridging the gap between color images and the human observation of scenes. *IEEE Trans. Image Process.* **2002**, *6*, 965–976. [CrossRef]

19. Ma, J.X.; Fan, X.N.; Ni, J.J.; Zhu, X.F.; Xiong, C. Multi-scale retinex with color restoration image enhancement based on Gaussian filtering and guided filtering. *Int. J. Mod. Phys. B* **2017**, *31*, 7. [CrossRef]

20. Ping, W.; Zhiwen, W.; Dong, L.; Canlong, Z.; Yuhang, W. Low Illumination Color Image Enhancement Based on Improved Retinex Theory. In Proceedings of the EITCE 2020: Proceedings of the 2020 4th International Conference on Electronic Information Technology and Computer Engineering, New York, NY, USA, 6–8 November 2020; pp. 334–339. [CrossRef]

21. Varghese, P.; Selva Saroja, G.A. Hexagonal image enhancement using Hex-Gabor filter for machine vision applications. *Mater. Today: Proc.* **2022**, *56*, 555–558. [CrossRef]

22. Chen, M.; Yu, L.; Zhi, C.; Sun, R.; Zhu, S.; Gao, Z.; Ke, Z.; Zhu, M.; Zhang, Y. Improved faster R-CNN for fabric defect detection based on Gabor filter with Genetic Algorithm optimization. *Comput. Ind.* **2022**, *134*, 103551. [CrossRef]

23. Wu, R.Q.; Yu, D.Y.; Liu, J.; Wu, H.; Chen, W.; Gu, Q.S. An improved fusion method for infrared and low-light level visible image. In Proceedings of the 14th IEEE International Computer Conference on Wavelet Active Media Technology and Information Processing (ICCWAMTIP), Chengdu, China, 15–17 December 2017; pp. 147–151.

24. Qiu, Y.H.; Tang, L.X.; Li, B.; Niu, S.L.; Niu, T.Z. Uneven Illumination Surface Defects Inspection Based on Saliency Detection and Intrinsic Image Decomposition. *IEEE Access* **2020**, *8*, 190663–190676. [CrossRef]

25. Zhang, J.W.; Wang, H.Y.; Tian, Y.; Liu, K. An accurate fuzzy measure-based detection method for various types of defects on strip steel surfaces. *Comput. Ind.* **2020**, *122*, 12. [CrossRef]

26. Liu, G.H.; Zheng, X.T. Fabric defect detection based on information entropy and frequency domain saliency. *Vis. Comput.* **2021**, *37*, 515–528. [CrossRef]

27. Wang, X. Laplacian Operator-Based Edge Detectors. *IEEE Trans. Pattern Anal. Mach. Intell.* **2007**, *29*, 886–890. [CrossRef]

28. Waheed, W.; Deng, G.; Liu, B. Discrete Laplacian Operator and Its Applications in Signal Processing. *IEEE Access* **2020**, *8*, 89692–89707. [CrossRef]

29. Meng, W.; Huisheng, Z.; He, H. A Pseudo Cross Bilateral Filter for Image Denoising Based on Laplacian Pyramid. In Proceedings of the 2008 IEEE International Symposium on Knowledge Acquisition and Modeling Workshop, Wuhan, China, 21–22 December 2008; pp. 235–238.

30. Kisacanin, B.; Schonfeld, D. A fast thresholded linear convolution representation of morphological operations. *IEEE Trans. Image Process.* **1994**, *3*, 455–457. [CrossRef]

31. Bernardino, A.; Santos-Victor, J. Fast IIR Isotropic 2-D Complex Gabor Filters With Boundary Initialization. *IEEE Trans. Image Process.* **2006**, *15*, 3338–3348. [CrossRef]

32. David, E.; Ungureanu, P.; Ansorge, M. A fast recursive implementation of Gabor filters. In Proceedings of the International Symposium on Signals, Circuits and Systems, 2005, ISSCS 2005, Iasi, Romania, 14–15 July 2005; Volume 2, pp. 581–584.

33.  Liu, X.; Pedersen, M.; Wang, R. Survey of natural image enhancement techniques: Classification, evaluation, challenges, and perspectives. *Digit. Signal Process.* **2022**, *127*, 103547. [CrossRef]

34.  Egiazarian, K.; Ponomarenko, M.; Lukin, V.; Ieremeiev, O. Statistical evaluation of visual quality metrics for image denoising. In Proceedings of the 2018 IEEE International Conference on Acoustics, Speech and Signal Processing (ICASSP), Calgary, AB, Canada, 15–20 April 2018; pp. 6752–6756.